Proc. Natl. Acad. Sci. USA
Vol. 96, pp. 10450–10455, August 1999
Neurobiology

Noise shaping in populations of coupled model neurons

D. J. Mar*†, C. C. Chow‡, W. Gerstner§, R. W. Adams¶, and J. J. Collins*

*Center for BioDynamics and Department of Biomedical Engineering, Boston University, Boston, MA 02215; ‡Department of Mathematics, University of Pittsburgh, Pittsburgh, PA 15260; §Center for Neuromimetic Systems, Swiss Federal Institute of Technology, Lausanne CH-1015, Switzerland; and ¶Analog Devices Corporation, Wilmington, MA 01887

Edited by Nancy J. Kopell, Boston University, Boston, MA, and approved June 23, 1999 (received for review March 23, 1999)

ABSTRACT **Biological information-processing systems, such as populations of sensory and motor neurons, may use correlations between the firings of individual elements to obtain lower noise levels and a systemwide performance improvement in the dynamic range or the signal-to-noise ratio. Here, we implement such correlations in networks of coupled integrate-and-fire neurons using inhibitory coupling and demonstrate that this can improve the system dynamic range and the signal-to-noise ratio in a population rate code. The improvement can surpass that expected for simple averaging of uncorrelated elements. A theory that predicts the resulting power spectrum is developed in terms of a stochastic point-process model in which the instantaneous population firing rate is modulated by the coupling between elements.**

An important issue in neuroscience is how neurons encode information (1–8). Here, we consider the problem of encoding an analog signal in the firing times of a population of neurons. Several factors must be accounted for in addressing this issue. First, the firing records of neurons are often noisy and irregular (8, 9). Second, cortical neurons sometimes fire relatively slowly compared to many of the signals they may need to encode (10, 11).

We explore a method for population rate coding by which a network of coupled noisy neurons can encode relatively high-frequency signals. We consider a system of N neurons that receive the same analog input. The relevant output is the population firing rate $F_N(t)$, the number of neuronal firings per unit time summed across the population. This quantity does not require averaging over a significant time window, and it can respond quickly to rapidly changing inputs (12–15). For neurons firing asynchronously, F_N is approximately N times the single-neuron rate. The input signal is encoded in the modulation of the firing times of the neurons in the network. When the analog input is converted to a train of discrete spike events, "quantization" noise from the errors made in digitization is unavoidable and limits the fidelity with which the output signal can be decoded. For N uncoupled, independent neurons, the quantization noise power grows as N, and the coherent signal power grows as N^2. The system signal-to-noise ratio (SNR), defined as the ratio of the output signal power to the noise power, grows as N. The SNR is improved if either the output signal is increased or the noise is reduced. Some systems are limited in the maximal signal power that they can process. In such cases, another important figure of merit is the system dynamic range (DR), which we take to be the ratio between the maximum signal power the system can tolerate and the noise power. For a fixed maximum output signal power, improving the DR is equivalent to reducing the noise. An example of a system requiring high DR is the human auditory system, which processes signals ranging from a soft whisper to a loud jet engine.

We propose a method to improve the DR and SNR for a population rate code beyond simple averaging over N independent elements. Inspiration for our method comes from the concept of noise shaping, used in certain electronic analog-to-digital converters (16). It has been proposed that noise shaping could be used in a single neuron (17–19); in this paper, we pursue this question for a network of coupled neurons. Our approach uses inhibitory coupling between neurons to generate temporal anticorrelations. In the frequency domain, these correlations shift the quantization noise power from one part of the spectrum to another, thereby "shaping" the spectrum and, more importantly, lowering the noise at the frequencies of interest. We are able to suppress the quantization noise power within the signal bandwidth at a rate of N^{-1}, and therefore, for a fixed operating range, increase the usable DR. We also find that, for sufficiently large coupled networks, the SNR improves as N^2.

Integrate-and-Fire (IF) Network

We model the neuronal network as a population of N IF oscillators. Each neuron is characterized by a voltage $V_i(t)$ and fires whenever V_i exceeds a threshold V_{th}. Each neuron is coupled to other neurons via a sum over postsynaptic currents γ. Between firings, the dynamics for V_i are given by

$$\frac{dV_i}{dt} = -\frac{V_i}{\tau_m} - \sum_{j=1}^{N} \sum_m K_{ij}\gamma(t - t_j^m) + \alpha_i I(t), \qquad [1]$$

where

$$\gamma(t') = e^{-t'/\tau_s}, \qquad t' > 0. \qquad [2]$$

In Eq. **1**, i and j index elements of the network ($i, j \in \{1, \ldots, N\}$), and t_j^m, $m = 1, 2, 3, \ldots$, is the set of firing times of the jth neuron. After firing, V_i is reset to a random value between 0 and $V_{\text{th}}\delta$, where $\delta = 0.75$ for all results shown, with the exception of Fig. 5. The postsynaptic current $\gamma(t')$ in Eq. **2** exponentially decays with time constant τ_s for $t' > 0$, and vanishes for $t' \leq 0$. Other possible postsynaptic current waveforms include α-functions, which have a finite rise time before decaying (20–22).

Eq. **1** describes the ith neuron as a leaky integrator of the total source current; this current consists of a driving term $I(t)$ common to all of the neurons and an interaction term $\Sigma_{j,m} K_{ij}\gamma(t - t_j^m)$ due to contributions whenever any neuron in the population has fired. In our sign convention, $K_{ij} > 0$ corresponds to inhibitory coupling. For simplicity, for all of the results shown here, the coupling is all-to-all: $K_{ij} = K$, a constant. Heterogeneity among the individual neuron rates is provided by a distribution in the values of the coefficients α_i. The time scales in this coupled-oscillator system are the

The publication costs of this article were defrayed in part by page charge payment. This article must therefore be hereby marked "*advertisement*" in accordance with 18 U.S.C. §1734 solely to indicate this fact.

PNAS is available online at www.pnas.org.

This paper was submitted directly (Track II) to the *Proceedings* office.
Abbreviations: SNR, signal-to-noise ratio; DR, dynamic range; IF, integrate-and-fire; ISI, interspike interval.
†To whom reprint requests should be addressed. E-mail: djmar@bu.edu.

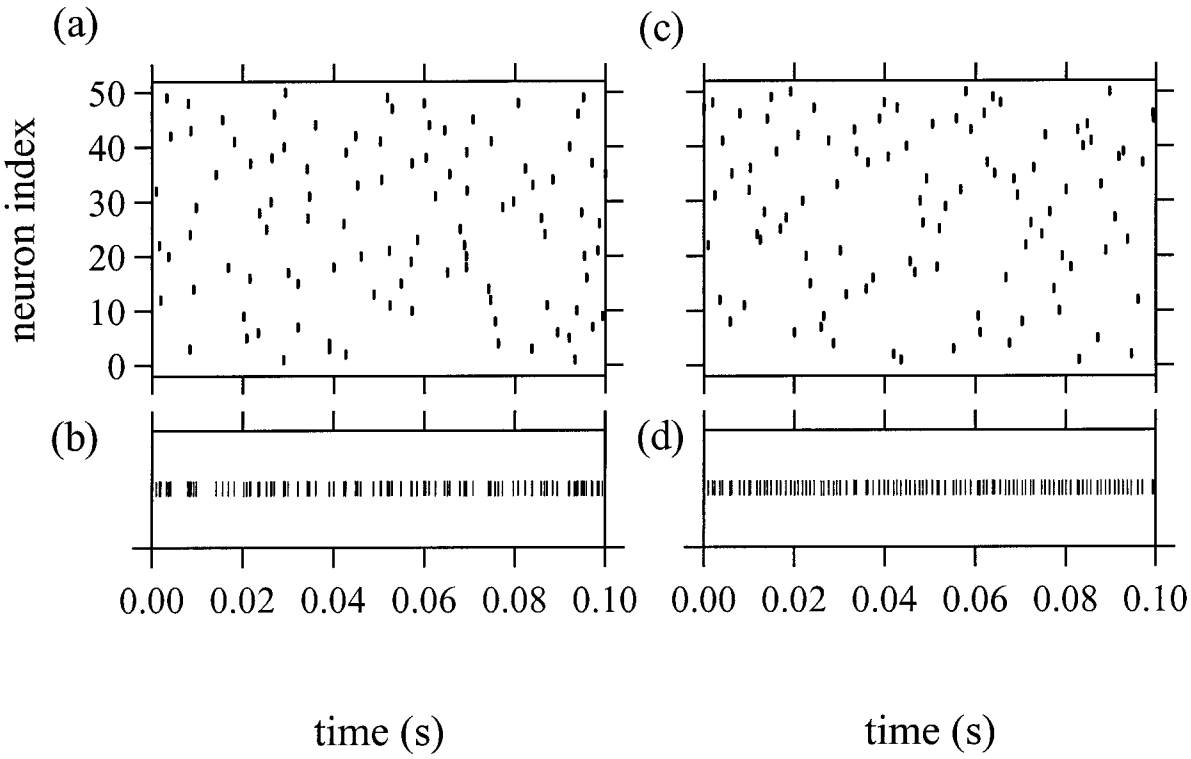

FIG. 1. Raster plots of the firing events for uncoupled (*a* and *b*) and coupled (*c* and *d*) networks of $N = 50$ elements (Eqs. **1** and **2**). The network heterogeneity α_i is uniformly distributed in the interval (1.27, 1.50), corresponding to the bottom and top of *a* and *c*, and the overall network firing rate in both cases is $F_N = 1.000 \times 10^3 \pm 1$ Hz. In *b* and *d*, the raster plots are collapsed into a collective record for the entire network. The membrane and synapse times are $\tau_m = 1$ s and $\tau_s = 10^{-3}$ s, respectively. The coupling strength and applied current, respectively, are $K = 0$ and $I_0 = 9.48$ (*a* and *b*) and $K = 50.0$ and $I_0 = 47.3$ (*c* and *d*).

membrane time $\tau_m = 1$ s and the synaptic time $\tau_s = 10^{-3}$ s (units have been assigned for convenience). The random reset introduces phase noise into each neuron whenever it fires. We remark that our model summarized in Eqs. **1** and **2** could possibly synchronize (23–28), particularly with inhibitory coupling (29–32). However, these synchronization effects are deliberately suppressed by the strong phase randomization from the random reset and the distribution in natural oscillator rates (33, 34).

Numerical Simulation Results

We numerically integrate (35) the above model and record the firing times of each neuron.‖ Fig. 1 shows raster plots of the firings in a network of $N = 50$ neurons. In Fig. 1 *a* and *b*, the network is uncoupled ($K = 0$), whereas in Fig. 1 *c* and *d*, the coupling between elements is inhibitory ($K = 50.0 > 0$). In both cases, the input $I(t)$ is a constant I_0, and the mean network firing rate is $F_N = 1{,}000 \pm 1$ Hz. In Fig. 1 *b* and *d*, we collapse the raster plots into network firing records to show the difference in the summed outputs. In particular, occasional clumps and gaps are observed in the output of the uncoupled network (see Fig. 1*b*), as expected for a set of uncorrelated elements. However, the record in Fig. 1*d* for the coupled network appears to be distributed relatively smoothly in time.

To quantify this, we show in Fig. 2*a* histograms of the interspike intervals (ISIs) corresponding to the network outputs shown in Fig. 1 *b* and *d*. Data are shown for trial durations of 200 s and using a bin width $\Delta = 0.1$ ms. The histogram decays exponentially in the uncoupled case with a time constant of approximately 1 ms, consistent with an uncorrelated Poisson process. In contrast, the histogram of the coupled network is narrowly distributed about its maximum at 1 ms, which is consistent with the "smooth" firing record in Fig. 1*d*.

The difference between coupled and uncoupled networks is further illustrated by the autocorrelation function $a(\tau)$ of the network firing sequences $X_N(t)$.** In Fig. 2*b*, $a(\tau)$ is plotted for time shifts $\tau < 5$ ms, using a sampling interval of 0.1 ms. For

‖The system is integrated using a fourth-order Runge–Kutta routine (35). Accuracy in the firing sequence is ensured by using an adaptive step size to handle nearly simultaneous firings. This scheme is not critical for obtaining our results. The system is integrated for 200 s after a settling period of 30 s.

**We compute $a(\tau) = \langle X_N(t')X_N(t' - \tau)\rangle$, where $X_N(t)$ is defined on a discrete set of times $k\Delta$, where k indexes the bin intervals. We set $X_N(t) = 1$ if there is a firing event between t and $t + \Delta$, and $X_N(t) = 0$ otherwise.

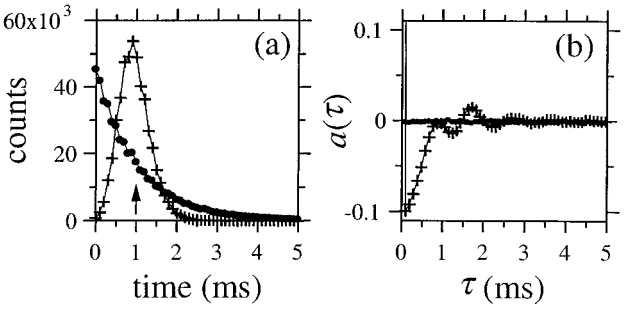

FIG. 2. (*a*) Histogram of ISIs for the collective firing output of the network (see Fig. 1 *b* and *d*) taken for trial durations of 200 s and a bin width of 0.1 ms. The inverse population rate $F_N^{-1} = 1.0$ ms is indicated by the arrow. (*b*) Autocorrelation of the collective firing record (see Fig. 1 *b* and *d*) taken for 200 s and using a sampling interval of 0.1 ms. For both *a* and *b*, dots (●) and crosses (+) represent data for the uncoupled and coupled networks, respectively. Lines between points are drawn to guide the eye.

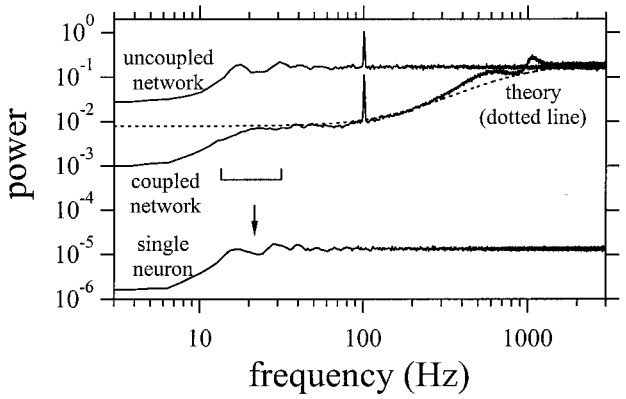

FIG. 3. Power spectra for a network of $N = 50$ neurons whose dynamics are given by Eqs. **1** and **2**. The top trace is for the uncoupled network ($K = 0$, $I_0 = 9.48$) and the middle trace is for a coupled network ($K = 50.0$, $I_0 = 47.3$). In both cases, the input signal current is $I(t) = I_0 + A \sin(2\pi f_0 t)$, where $f_0 = 100$ Hz and $A = 2.365$. Other system parameters are as specified in the caption of Fig. 1. In the coupled case, the lower quantization noise below $f_c = 800$ Hz corresponds to larger DR. The measured SNR at f_0 is 8.1 dB in the uncoupled network and 10.6 dB in the coupled network. The scale bar between 12 and 28 Hz indicates the range of individual neuron firing rates in the coupled network. The dotted line is the theoretical prediction from Eq. **7**. The bottom trace is the spectrum for a single representative neuron selected from the coupled network. The mean firing rate of this neuron is 19 Hz (see arrow).

the uncoupled network, $a(0) = 1$ and $a(\tau)$ is essentially 0 thereafter, indicative of uncorrelated firing. With inhibitory coupling, $a(\tau)$ is negative immediately after $\tau = 0$, crosses 0 at $\tau \approx 0.8$ ms, and then displays decaying oscillations with a period of approximately 1 ms. This describes a system with anticorrelated firing. After a neuron fires, the inhibitory coupling forces the network to wait approximately 0.8 ms before the next neuron can fire.

Fig. 3 shows power spectra on logarithmic axes for the uncoupled and coupled networks.†† For these data, we have included in the applied current $I(t)$ a sinusoidal input signal term $S(t) = A \sin(2\pi f_0 t)$ with frequency $f_0 = 100$ Hz and amplitude $A = 2.365$. The sinusoidal signal is clearly visible above the background for both cases and does not display much broadening or other nonlinear distortion. The inhibition lowers the overall firing activity of every neuron. To make a meaningful comparison between the two cases, we compensate for this effect by adjusting the dc component I_0 of the applied current to maintain the population rate F_N at 1,000 ± 1 Hz.

For the uncoupled network, the spectrum is flat over most of the frequency range shown, consistent with the vanishing autocorrelation in Fig. 2*b*. This behavior is a direct result of asynchronous firing because of the random reset, the heterogeneity in α_i, and, most importantly, the lack of any interneuron interactions. The decrease in the spectrum below about 15 Hz is caused by the refractory time of the individual neurons (36, 37).

When the neurons are coupled by inhibition, both signal and noise power are reduced from their values in the uncoupled network. As shown in Fig. 3, the noise power is significantly suppressed over a wide frequency range, up to approximately $f_c = 800$ Hz. Immediately below this "corner" frequency, the noise power varies as f^2 and decreases to a maximum suppression of >13 dB at frequencies <80 Hz. The power at low frequencies is transferred partially to frequencies around f_c. This power is visible in Fig. 3 as a small bump near f_c and F_N.

In Fig. 3, the bandwidth over which the noise is suppressed is free from peaks (except the input signal at f_0) and other structure. This reflects the absence of synchronization between the network elements (also visible in Fig. 1*c*) and underscores the asynchronous firing nature of the network. We also show in Fig. 3 a spectrum obtained from a single representative neuron in the coupled network. This neuron possesses an intrinsic rate of 19 Hz (see arrow), near the network average. The single-neuron spectrum is flat over a wide bandwidth, except for suppression below 20 Hz because of refractoriness. The absence of a peak or other feature at f_0 implies that this single neuron by itself does not carry any information at the signal frequency. The noise-shaping and signal-transmission characteristics are network properties.

Noise shaping is a dynamical effect between neurons firing near their intrinsic rates. Each neuron's rate is suppressed slightly by the mean network activity. The coupling disfavors short ISIs in the network record and spaces out the firing events, as shown in Figs. 1 and 2. We emphasize that this shaping takes place at frequencies both below and above the firing rates of the individual neurons. The fastest neuron in the coupled network fires at 28 Hz (see bar in Fig. 3), less than twice the nominal single-element rate $F_N/N = 20$ Hz and well below the corner frequency f_c.

To illustrate how the noise-shaping effect varies with population size, we first show in Fig. 4*a* the dependence of the population rate F_N on N. Both axes are scaled by τ_s. For these data, $I_0 = 47.3$, $K = 50.0$, and all other network parameters are the same as in Figs. 1–3. The data for $\tau_s = 0.3$, 1, 3, and 10 ms all fall near the same curve, indicating that the maximum output rate, and hence f_c, is directly dependent on the product $N\tau_s$. In addition, the inverse synapse time τ_s^{-1} specifies an upper limit on f_c. As seen in Fig. 4*a*, for small N, $F_N\tau_s$ increases with N. In this regime, the ISIs are much larger than τ_s, and F_N scales linearly with N. As the size of the network grows, the ISIs decrease toward τ_s. The individual firing rates become increasingly slowed by the synaptic inhibition, and the population rate increases only slightly thereafter. For our choices of parameters, F_N and f_c saturate for $N\tau_s \gtrsim 20$ ms.

We next show how adding more neurons to the network confers beneficial effects for the DR and the SNR. In Fig. 4*b*, we show a log–log plot of the quantization noise power P measured at 100 Hz (●) and 30 Hz (open symbols), as N varies. For these data, $\tau_s = 1$ ms, $I_0 = 47.3$, and $A = 0$. Squares represent P at 30 Hz for $K = 0$; as expected, P increases linearly with N for the uncoupled network. Circles in Fig. 4*b* show P for $K = 50$. For the coupled network, P decreases approximately as N^{-1} for large N; in this regime, $F_N\tau_s \approx 1$, and the coupling effectively narrows the histogram in Fig. 2*a* and shapes the spectrum. The decrease in noise power results in a significant increase in system DR. However, this improvement does not extend to arbitrarily large N. For very large values of $N\tau_s$, neurons with small α_i receive so much inhibition that they are prevented from reaching threshold and firing.

The network SNR is also enhanced by the coupling. In Fig. 3, the measured SNR is improved by 2.5 dB. In Fig. 4*c*, we show the SNR measured for an input signal at $f_0 = 30$ Hz, just above the fastest individual neuron rate. For $N \gtrsim 15$, the SNR improves approximately as N^2, faster than that for simple averaging. Clearly, there is a large region in parameter space in which the coupled network significantly outperforms simple averaging in its DR and SNR.

Theory

The spectrum shown in Fig. 3 can be estimated analytically by treating the population activity as a modulated stochastic point process. The spectrum can then be computed rigor-

††For the (one-sided) spectra shown in Fig. 3, the data are partitioned into 255 overlapping sequences and windowed using a Bartlett window. The results presented herein are not sensitive to the details of the Fourier transform segmentation or the choice of window.

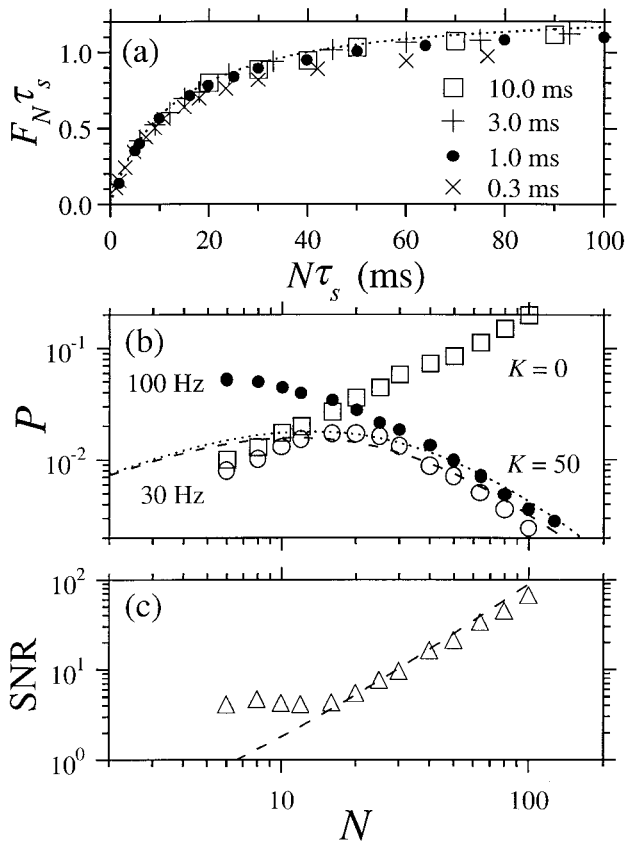

FIG. 4. Dependence of network firing behavior on the population size N. (*a*) Population firing rate F_N vs. N, where both axes have been scaled by τ_s. The network parameters are identical to those in Figs. 1–3, with the exception of N and τ_s. ×, ●, +, and □ represent data for τ_s = 0.3, 1, 3, and 10 ms, respectively. The dotted line is the theoretical rate obtained from Eq. **6**. (*b*) Log–log plot of measured quantization noise power P at 100 Hz (●) and 30 Hz (open symbols) vs. N, taken with τ_s = 1 ms, $I_0 = 47.3$, $A = 0$, and other parameters as in Figs. 1–3. Squares and circles represent data for uncoupled ($K = 0$) and coupled ($K = 50$) networks, respectively. (*c*) Log–log plot of SNR vs. N measured at $f = 30$ Hz for a network with $K = 50$ and $A = 2.365$. In *b* and *c*, theoretical predictions obtained from Eqs. **6** and **7** for the coupled networks are shown by a dotted line ($f = 100$ Hz) and dashed lines ($f = 30$ Hz), respectively.

ously for certain classes of noise intensity (38, 39; C.C.C. and W.G., unpublished data). Here we give a simple heuristic derivation. For an uncoupled network whose elements fire randomly, the average of the population firing rate F_N depends on the sum of all of the applied currents. With coupling, F_N is modulated, and for a finite N, fluctuates around the mean. We define the population activity (33) as $F(t) = \sum_{j=1}^{N} \sum_m \delta(t - t_j^m)$. The time average of $F(t)$ is the mean population firing rate, because $\langle F(t)\rangle = (1/T)\int_0^T F(t)dt = n/T$, where n is the number of firings in the time interval T. For nearly asynchronous firing as observed in our simulations, we can assume that $F(t)$ represents the population firing rate, including fluctuations (33).

To calculate the spectrum, we first consider the effects on a single neuron. In our simulations, $\tau_m \gg \tau_s$, so we consider the limit of no leakage. Because the coupling $K_{ij} = K$ is uniform and all-to-all, we can simplify the coupling term in Eq. **1**. The dynamics of a single neuron obeys

$$\frac{dV_i}{dt} \simeq -K\int_0^\infty \gamma(t')F(t-t')dt' + \alpha_i[I_0 + S(t)] + \tilde{\xi}(t), \quad \textbf{[3]}$$

where $\gamma(t')$ is given in Eq. **2**, I_0 and $S(t)$ are the mean (dc) and time-varying components of $I(t)$, and $\tilde{\xi}(t)$ is a stochastic forcing term that mimics the random effects. For nearly asynchronous firing, the voltage in Eq. **3** grows approximately linearly with t. The firing rate of neuron i is then proportional to dV_i/dt. We obtain the population rate by normalizing by the effective threshold voltage $V_{\text{eff}} = V_{\text{th}}(1 - \delta/2)$‡‡ and summing over elements: $F(t) \simeq V_{\text{eff}}^{-1}\sum_{i=1}^{N} dV_i/dt$. Using Eq. **3** in this expression yields a stochastic equation for the population rate:

$$F(t) \simeq \frac{N}{V_{\text{eff}}}\left[\bar{I} - K\int_0^\infty \gamma(t')F(t-t')dt' + \bar{S}(t)\right] + \xi(t), \quad \textbf{[4]}$$

where $\bar{I}$ and $\bar{S}(t)$ are the network-averaged dc and time-dependent inputs, $\xi(t)$ is uncorrelated white noise with zero mean and variance $\langle\xi(t)\xi(t')\rangle = \sigma^2\delta(t - t')$, and $\sigma^2 \approx F_N\Delta$ is obtained under the assumption that the firings can be modeled as a Poisson process.§§ The coupling and random reset cause fluctuations around the mean rate. Let $F(t) = F_N + \delta F(t)$, where F_N is the mean firing rate and $\delta F(t)$ is a fluctuation around F_N. Eq. **4** then becomes

$$F_N + \delta F(t) \simeq \frac{N}{V_{\text{eff}}}\left[\bar{I} - K\tau_s F_N - K\int_0^\infty \gamma(t')\delta F(t-t')dt' + \bar{S}(t)\right] + \xi(t). \quad \textbf{[5]}$$

From the time-independent terms in Eq. **5**, the mean firing rate is then obtained as

$$F_N = \frac{N\bar{I}}{V_{\text{eff}} + NK\tau_s}. \quad \textbf{[6]}$$

We can define a critical network size $N_c = V_{\text{eff}}(K\tau_s)^{-1}$, above which F_N begins to saturate. Using the values $\bar{I} \approx 65.5$, $N = 50$, $V_{\text{eff}} = V_{\text{th}}(1 - \delta/2) = 0.625$, $K = 50$, and $\tau_s = 10^{-3}$, we obtain $F_N = 1.05$ kHz, in good agreement with the simulations. We also plot the relation in Eq. **6** in Fig. 4*a* and see that it agrees well with the numerical results.

The spectrum of the noise fluctuations is obtained from the time-varying terms in Eq. **5** as the absolute square of the Fourier transform of $\delta F(t)$:

$$P(f) = \langle|\delta F(f)|^2\rangle = \frac{\sigma^2 + N^2V_{\text{eff}}^{-2}\hat{S}^2(f)}{|1 + NKV_{\text{eff}}^{-1}\hat{\gamma}(f)|^2}, \quad \textbf{[7]}$$

where $\hat{\gamma}(f) = 1/(\tau_s^{-1} - 2\pi if)$ is the Fourier transform of the postsynaptic current γ in Eq. **2** and f is the frequency. The coupling kernel $\hat{\gamma}(f)$ has a cutoff at $2\pi f = \tau_s^{-1}$. For sufficiently large N and K and at sufficiently low frequency $NKV_{\text{eff}}^{-1}\hat{\gamma}(f) \gg 1$ and the coupling "shapes" the spectrum of both signal and noise. The theoretically predicted spectrum in Eq. **7** using the same parameter values as above with $\Delta = 0.1$ ms is compared to the data for the coupled network in Fig. 3. The dotted line has no free parameters. As shown, the theory agrees well with the data in matching the corner frequency f_c and also provides a good estimate of the noise-shaping level below f_c. In Fig. 4*b*, we have plotted the calculated noise power at $f = 100$ Hz (dotted line) and $f = 30$ Hz (dashed line), from

‡‡At each firing event, the neuron is reset to a random value between 0 and $V_{\text{th}}\delta$. On average, this reduces the potential difference from the threshold by $V_{\text{th}}\delta/2$.

§§The probability of a firing event during an interval of duration Δ is $F_N\Delta$. In this case, the noise power is the variance in the bin occupation, or $\sigma^2 = F_N\Delta(1 - F_N\Delta)$. For small Δ, this approaches the Poisson result $\sigma^2 = F_N\Delta$. For the data in Fig. 3, σ^2 agrees with the Poisson prediction to within 1%.

Eqs. **6** and **7**. As shown, the theory matches the numerical data well for $N \gtrsim 30$.

From Eq. **7**, we see that SNR $= N^2\hat{S}^2(f)/(V_{\text{eff}}^2\sigma^2)$. There are two regimes for the SNR, depending on whether $N > N_c$. For small networks, ($N \ll N_c$), σ^2 scales as N and SNR $\propto N$, similar to simple averaging. As N is increased beyond N_c, the population rate F_N, and hence σ^2, saturates. Then SNR $\propto N^2$. This regime is seen in Fig. 4*c*, in which the dotted line shows the calculated SNR from Eq. **7**. Again, the agreement is excellent for $N > N_c = 12.5$.

Deviations from the theory likely occur because the firing rates of the individual neurons possess nonlinearities and correlations that deviate from a pure Poisson process. For example, the theory does not reproduce the oscillations in the autocorrelation function (see Fig. 2); in the noise spectrum, these are manifest as a bump in Fig. 3 near f_c. The theoretical value from Eq. **7** for $P(f = 100$ Hz) underestimates the numerical data for small N (see dots and dotted line in Fig. 4). In this regime, f is comparable to f_c, and the data reflect the noise power in the nearby bump. We have also ignored the intrinsic refractory time of the neurons caused by the IF dynamics. As seen in Fig. 3, and also shown previously (37), refractoriness alone leads to noise-shaping. We therefore expect Eq. **7** to overestimate the spectrum at very low frequencies.[¶¶] This is also seen in Fig. 4*b* by comparing theory (dashed line) and data (circles) for $P(f = 30$ Hz) for $N \leq 10$.

Summary and Conclusions

Our results demonstrate improved signal encoding through noise shaping in a network of coupled model neurons. Noise shaping allows the population to encode signals over a wide bandwidth with extended DR and improved SNR. By firing nearly asynchronously, the network can encode signals with frequencies well above those of the individual elements. Because coupling lowers the quantization noise power, for a given SNR, analog signals may be encoded with fewer neurons. This remains true even when the population firing rate is unchanged. In our model, the elements interact via a coupling rule that is local in time and hence is easy to implement. Noise and heterogeneity in the network help serve to break up clustering and stabilize the asynchronous firing state. They may also be used to boost weak signals above threshold (40–44).

The DR and SNR both improve with increasing N at rates faster than that of an uncoupled network. The inhibitory coupling shapes the spectrum and reduces the noise power at low frequencies; this reduction results directly in an improved DR. However, the shaping also reduces the signal power accordingly. The SNR is improved by a different effect: the inhibition sets a maximum population firing rate that is determined by the synaptic time scale, the applied current, and the coupling constant. As the coupled network is increased beyond a critical N, the background noise power, which is proportional to F_N, saturates while the signal power continues to grow as N^2. This increase in SNR could be observed in any network in which the inhibitory coupling reduces the population rate. These dependences of DR and SNR surpass those of an uncoupled network, for which the noise power increases linearly with N.

In our simulations, we have found that the noise-shaping effect shown in Fig. 3 is robust against element heterogeneity among the input coefficients α_i and against variations in the coupling coefficients K_{ij}. We have also been able to generate more complicated noise-shaped spectra, such as a notch at a given frequency as shown in Fig. 5, by suitable choices for the postsynaptic current waveform $\gamma(t)$. We also note that shaping need not be limited to anticorrelations between individual spikes. For instance, it could take place between neuron bursts. With different network architectures, it may be possible to create noise-shaping networks in which the SNR, DR, or other performance criteria are significantly enhanced beyond what is shown here.

[¶¶] As $f \to 0$, the ratio of $P(f)$ for the coupled network to that of the uncoupled network approaches 0.04, or 14 dB, for the parameters used in Fig. 3. This agrees well with the noise suppression measured at the left edge of the figure.

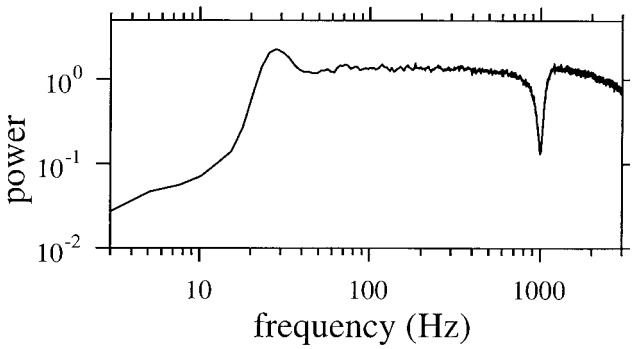

FIG. 5. Power spectrum for a network of $N = 40$ neurons, coupled with the synaptic kernel $\gamma(t') = \cos(2\pi t'/T)\exp(-t'/\tau_s)$, with $T = 1.0$ ms and $\tau_s = 5.0$ ms. Other parameters are $I_0 = 15.4$, $K = -15$, and $\delta = 0.5$, and α_i is uniformly distributed between 1.0 and 1.5.

In biological experiments, noise shaping may be difficult to detect in the firing records of individual neurons. These records may look Poisson-like and, except for refractoriness, display few correlations. In particular, cross-correlations between pairs of neurons in simulations of the coupled network do not show significant anticorrelations (data not shown). Noise shaping arises from the correlations in the aggregate firings, a collective property of the population. A demonstration of noise shaping in biological systems would require the simultaneous recording of the firings from many coupled neurons (45, 46). Such demonstrations are of interest because noise shaping or a variant thereof may be at work in biological systems that operate at frequencies higher than those of the network elements (11, 47).

We thank N. Kopell for a critical reading of the manuscript. This work was supported at Boston University by a contribution from Ray Stata of Analog Devices, Inc., and by National Institute of Mental Health Grant K01 MH01508 (C.C.C.).

1. Shadlen, M. N. & Newsome, W. T. (1994) *Curr. Opin. Neurobiol.* **4,** 569–579.
2. Sejnowski, T. J. (1995) *Nature (London)* **376,** 21–22.
3. Softky, W. R. (1995) *Curr. Opin. Neurobiol.* **5,** 239–247.
4. Singer, W. & Gray, C. M. (1995) *Annu. Rev. Neurosci.* **18,** 555–586.
5. Ferster, D. & Spruston, N. (1995) *Science* **270,** 756–757.
6. Stevens, C. F. & Zador, A. (1995) *Curr. Biol.* **5,** 1370–1371.
7. Meister, M. (1996) *Proc. Natl. Acad. Sci. USA* **93,** 609–614.
8. Shadlen, M. N. & Newsome, W. T. (1998) *J. Neurosci.* **18,** 3870–3896.
9. Softky, W. R. & Koch, C. (1993) *J. Neurosci.* **14,** 334–350.
10. Thorpe, S., Fize, D. & Marlot, C. (1996) *Nature (London)* **381,** 520–522.
11. Carr, C. E. (1993) *Annu. Rev. Neurosci.* **16,** 223–243.
12. Tsodyks, M. V. & Sejnowski, T. (1995) *Network* **6,** 111–124.
13. van Vreeswijk, C. & Sompolinsky, H. (1996) *Science* **274,** 1724–1726.
14. Berry, M. J., II, & Meister, M. (1998) *J. Neurosci.* **18,** 2200–2211.
15. Gerstner, W. (1998) in *Pulsed Neural Networks*, eds. Maass, W. & Bishop, C. M. (MIT Press, Cambridge, MA), pp. 261–295.
16. Norsworthy, S. R., Schreier, R. & Temes, G. C., eds. (1997) *Delta-Sigma Data Converters* (IEEE Press, Piscataway, NJ).
17. Shin, J. H., Lee, K. R. & Park, S. B. (1993) *Int. J. Electronics* **74,** 359–368.

18. Cheung, K. F. & Tang, P. Y. H. (1993) *Proc. 1993 IEEE Int. Conf. Neural Networks*, 489–493.
19. Adams, R. W. (1997) *Proc. 1997 IEEE Int. Conf. Neural Networks*, 953–958.
20. Rall, W. (1967) *J. Neurophysiol.* **30,** 1138.
21. Traub, R. D. & Miles, R. (1991) *Neuronal Networks of the Hippocampus* (Cambridge Univ. Press, Cambridge, U.K.).
22. Tsodyks, M., Mitkov, I. & Sompolinsky, H. (1993) *Phys. Rev. Lett.* **71,** 1280–1283.
23. Mirollo, R. E. & Strogatz, S. H. (1990) *SIAM J. Appl. Math.* **50,** 1645–1662.
24. Kuramoto, Y. (1991) *Physica D* **50,** 15–30.
25. Hansel, D., Mato, G. & Meunier, C. (1995) *Neural Comput.* **7,** 307–337.
26. Gerstner, W., van Hemmen, J. L. & Cowan, J. D. (1996) *Neural Comput.* **8,** 1653–1676.
27. Chow, C. C. (1998) *Physica D* **118,** 343–370.
28. Bressloff, P. C. & Coombes, S. (1998) *Phys. Rev. Lett.* **81,** 2168–2171.
29. Wang, X. J. & Rinzel, J. (1992) *Neural Comput.* **4,** 84–97.
30. van Vreeswijk, C., Abbott, L. & Ermentrout, G. B. (1994) *J. Comp. Neurosci.* **1,** 313–321.
31. Terman, D., Kopell, N. & Bose, A. (1998) *Physica D* **117,** 241–275.
32. White, J. A., Chow, C. C., Ritt, J., Soto-Treviño, C. & Kopell, N. (1998) *J. Comp. Neurosci.* **5,** 5–16.
33. Gerstner, W. (1995) *Phys. Rev. E* **51,** 738–758.
34. Abbott, L. F. & van Vreeswijk, C. (1993) *Phys. Rev. E* **48,** 1483–1490.
35. Press, W. H., Teukolsky, S. A., Vetterling, W. T. & Flannery, B. P. (1992) *Numerical Recipes in C: The Art of Scientific Computing* (Cambridge Univ. Press, Cambridge, U.K.).
36. Edwards, B. W. & Wakefield, G. H. (1993) *J. Acoust. Soc. Am.* **93,** 3353–3364.
37. Spiridon, M., Chow, C. C. & Gerstner, W. (1998) in *Proceedings of the International Conference on Artificial Neural Networks (ICANN'98)*, eds. Niklasson, L., Boden, M. & Ziemke, T. (Springer, Berlin), pp. 337–342.
38. Hawkes, A. G. (1971) *Biometrika* **58,** 83–90.
39. Daley, D. & Vere-Jones, D. (1988) *An Introduction to the Theory of Point Processes* (Springer, New York).
40. Moss, F., Pierson, D. & O'Gorman, D. (1994) *Int. J. Bifurc. Chaos* **4,** 1383–1397.
41. Wiesenfeld, K. & Moss, F. (1995) *Nature (London)* **373,** 33–36.
42. Collins, J. J., Chow, C. C. & Imhoff, T. T. (1995) *Nature (London)* **376,** 236–238.
43. Pei, X., Wilkens, L. & Moss, F. (1996) *Phys. Rev. Lett.* **77,** 4679–4682.
44. Gammaitoni, L., Hänggi, P., Jung, P. & Marchesoni, F. (1998) *Rev. Mod. Phys.* **70,** 223–287.
45. Wilson, M. A. & McNaughton, B. L. (1993) *Science* **261,** 1055–1058.
46. Meister, M., Pine, J. & Baylor, D. A. (1994) *J. Neurosci. Methods* **51,** 95–106.
47. Gerstner, W., Kempter, R., van Hemmen, J. L. & Wagner, H. (1996) *Nature (London)* **383,** 76–78.